NeuroImage 227 (2021) 117647

Contents lists available at ScienceDirect

NeuroImage

journal homepage: www.elsevier.com/locate/neuroimage

Intrinsic functional clustering of ventral premotor F5 in the macaque brain

Saloni Sharma [a,b,*], David J. Schaeffer [d], Kasper Vinken [b,g], Stefan Everling [e,f], Koen Nelissen [b,c,**]

[a] Department of Neurobiology, Harvard Medical School, 220 Longwood Avenue, Boston, MA 02115, USA
[b] Laboratory for Neuro- & Psychophysiology, Department of Neurosciences, KU Leuven, O&N2 Campus Gasthuisberg, Herestraat 49, bus 1021, 3000 Leuven, Belgium
[c] Leuven Brain Institute, KU Leuven, 3000 Leuven, Belgium
[d] Department of Neurobiology, University of Pittsburgh, PA 15261, USA
[e] Centre for Functional and Metabolic Mapping, Robarts Research Institute, University of Western Ontario, London, Ontario, Canada
[f] Department of Physiology and Pharmacology, University of Western Ontario, London, Ontario N6A 5B7, Canada
[g] Harvard Medical School, Boston Children's Hospital, Boston, MA 02115, USA

ARTICLE INFO

Keywords:
Macaque monkey
Resting-state fMRI
Premotor

ABSTRACT

Neurophysiological and anatomical data suggest the existence of several functionally distinct regions in the lower arcuate sulcus and adjacent postarcuate convexity of the macaque monkey. Ventral premotor F5c lies on the postarcuate convexity and consists of a dorsal hand-related and ventral mouth-related field. The posterior bank of the lower arcuate contains two additional premotor F5 subfields at different anterior-posterior levels, F5a and F5p. Anterior to F5a, area 44 has been described as a dysgranular zone occupying the deepest part of the fundus of the inferior arcuate. Finally, area GrFO occupies the most rostral portion of the fundus and posterior bank of inferior arcuate and extends ventrally onto the frontal operculum. Recently, data-driven exploratory approaches using resting-state fMRI data have been suggested as a promising non-invasive method for examining the functional organization of the primate brain. Here, we examined to what extent partitioning schemes derived from data-driven clustering analysis of resting-state fMRI data correspond with the proposed organization of the fundus and posterior bank of the macaque arcuate sulcus, as suggested by invasive architectonical, connectional and functional investigations. Using a hierarchical clustering analysis, we could retrieve clusters corresponding to the dorsal and ventral portions of F5c on the postarcuate convexity, F5a and F5p at different antero-posterior locations on the posterior bank of the lower arcuate, area 44 in the fundus, as well as part of area GrFO in the most anterior portion of the fundus. Additionally, each of these clusters displayed distinct whole-brain functional connectivity, in line with previous anatomical tracer and seed-based functional connectivity investigations of F5/44 subdivisions. Overall, our data suggests that hierarchical clustering analysis of resting-state fMRI data can retrieve a fine-grained level of cortical organization that resembles detailed parcellation schemes derived from invasive functional and anatomical investigations.

1. Introduction

In recent years, resting-state fMRI (RS-fMRI) has come forward as a promising technique for investigating the functional organization of cortex non-invasively. For instance, data-driven clustering techniques using resting-state fMRI data have been used to examine the functional organization of the human brain, as well as the brains of non-human primates including macaques and marmosets (Goulas et al., 2012; 2017; Hutchison et al., 2012b; Hutchison and Everling, 2014; Vijayakumar et al., 2018; Schaeffer et al., 2019a, 2019b). As opposed to seed-based resting-state fMRI analyses, where a seed is defined a priori, usually based on some anatomical and/or functional criteria (Hutchison et al., 2012a; Babapoor-Farrokhran et al., 2013; Sharma et al., 2019), these data-driven approaches are independent of predefined structural/functional demarcations as functional connectivity itself is used to extract clusters in the brain.

So far, several resting-state fMRI studies that have used data-driven clustering techniques to examine the organization of the macaque frontal lobe have shown good correspondence with previously established parcellation schemes based upon invasive evidence (Goulas et al., 2017; Hutchison and Everling, 2014; Vijayakumar et al., 2018). However, these studies, focusing on the entire prefrontal cortex, including the arcuate sulcus and adjacent convexity (Hutchison and Everling, 2014), or the entire frontal cortex extending rostrally from the

* Corresponding author: Department of Neurobiology, Harvard Medical School, 220 Longwood Avenue, Boston, MA 02115, USA.
** Corresponding author: Lab for Neuro- & Psychophysiology, Department of Neurosciences, KU Leuven, O&N2 Campus Gasthuisberg, Herestraat 49, bus 1021, 3000 Leuven, Belgium.
E-mail addresses: Saloni_Sharma@hms.harvard.edu (S. Sharma), Koen.Nelissen@kuleuven.be (K. Nelissen).

https://doi.org/10.1016/j.neuroimage.2020.117647
Received 17 November 2020; Accepted 4 December 2020
Available online 15 December 2020

central sulcus (Goulas et al., 2017; Vijayakumar et al., 2018), have not demonstrated a similar fine-grained organization of the postarcuate sulcus as suggested by invasive functional and anatomical investigations of this region.

For instance, cyto- and myelo-architectonic examinations have suggested that the rostral portion of the ventral premotor cortex, area F5 (Rizzolatti and Luppino, 2001), located in the posterior bank of the lower arcuate and adjacent post-arcuate convexity, contains three subfields (Nelissen et al., 2005; Belmalih et al., 2009). While F5c is located on the posterior convexity of the lower arcuate sulcus, the posterior bank of the lower arcuate contains two more cyto-architectonically distinct F5 subfields at different posterior-anterior levels, F5p and F5a. In between premotor F5a in the posterior bank of the lower arcuate and prefrontal area 45B in the anterior bank, a dysgranular transition zone has been described, corresponding to area 44 (Petrides et al., 2005; Belmalih et al., 2009; Frey et al., 2014). Antero-ventrally, areas 44, F5a and F5c are bordered by another area with distinct cytoarchitectonic features, area GrFO (Gerbella et al., 2016; part of area ProM in Petrides et al., 2005), which occupies the anterior tip of the fundus and posterior bank of the arcuate and extends onto the frontal operculum.

Besides these architectonic studies, electrophysiological investigations examining the functional properties of neurons in/near the lower arcuate also confirm the presence of several distinct functionally specialized fields in this portion of cortex. From a motor point of view, F5p is primarily associated with hand-related motor acts, while F5c shows a dorsal to ventral transition from hand- to mouth-related motor responses, which overlap considerably (Gentilucci et al., 1988; Rizzolatti et al., 1988; di Pellegrino et al., 1992; Murata et al., 1997; Ferrari et al., 2003, 2017; Nelissen and Vanduffel, 2011; Maranesi et al., 2012; Shepherd and Freiwald, 2018; Sharma et al., 2019). Functional investigations of F5a suggest this subfield also plays a role in visually-guided hand grasping and encoding 3D shape information (Joly et al., 2009; Theys et al., 2012). Neuronal responses in the fundus of the arcuate (area 44) have so far mostly been associated with mouth motor acts such as jaw movements or vocalizations (Hage and Nieder, 2015; Petrides et al., 2005). While a detailed functional investigation of area GrFO is still lacking, single unit recordings suggest an involvement in the execution of both hand and mouth actions (Ferrari et al., 2003, 2005).

Here, by focusing specifically on the fundus/posterior bank of the lower arcuate sulcus and adjacent convexity of the macaque monkey, we examined to what degree data-driven resting-state clustering parcellations resemble organizational schemes derived from architectonical, connectional and/or functional investigations, as outlined above. Hierarchical clustering analysis was performed on resting-state fMRI data collected from a group of eight awake rhesus monkeys. To further corroborate these data-driven topologies, we also conducted voxel-wise seed-based functional connectivity analyses using the clusters obtained from the hierarchical clustering analysis. This allowed us to examine the unique functional connectivity profile for each of these clusters and to compare this to previous tract-tracing investigations (Frey et al., 2014; Gerbella et al., 2016, 2011) and model-based seed-based resting-state analysis (Neubert et al., 2014; Sharma et al., 2019) obtained from each of these cortical subfields.

2. Materials and methods

2.1. Subjects

Eight monkeys participated in the awake resting-state fMRI experiments (monkeys M1 – M8, *Macaca mulatta*, 6 male, 2 female, 5–8 kgs). All experimental and animal care procedures followed national and Europeans guidelines and were approved by the animal ethical committee of KU Leuven.

2.2. Awake resting-state fMRI

A single fMRI resting-state run lasted for 300 volumes during which the monkeys had to fixate at a red dot in the center of a screen in front of them while getting juice rewards for maintaining fixation. Similar tasks requiring subjects to fixate on a target have also been used in other monkey (Mantini et al., 2011) or human resting-state studies (Agcaoglu et al., 2019; Patriat et al., 2013; Wang et al., 2010). Although the specific condition may have an impact on overall resting-state fMRI activity, requiring subjects to fixate has been shown to result in less variability between subjects and greater reliability of within-network connectivity compared to tasks not requiring fixation (Agcaoglu et al., 2019; Patriat et al., 2013).

Data were acquired using a gradient-echo T2*-weighted echo-planar imaging sequence of 40 horizontal slices (TR = 2 s, TE = 17 ms, flip angle = 90°, 1.25 mm isotropic) in a Siemens 3T full body scanner. For data acquisition, we used an in-house designed and manufactured eight-channel phased array coil, and a saddle shaped, radial transmit-only surface coil (Kolster et al., 2009). An iron contrast agent (Molday ION, BioPAL in Monkey M1-M4 and MION; Sinerem, Laboratoire Guerbet in Monkey M5-M8) was injected intravenously (6 – 12 mg/kg) before each scanning session to improve signal-to-noise ratio (Vanduffel et al., 2001). For the resting-state fMRI data, runs with a fixation performance below 85% were not included for data analysis. Furthermore, the average correlation across voxel time-series was calculated for each run. Those runs with a value below or above two times the median across runs were considered artifactual and were excluded from further analysis (Mantini et al., 2011; Sharma et al., 2019). This resulted in 18 runs from monkey M1, 19 runs from monkey M2, 17 runs from monkey M3, 19 runs from monkey M4, 18 runs from monkey M5, 14 runs from monkey M6, 15 runs from monkey M7 and 19 runs from monkey M8. The awake resting-state data in this study are the same as in a previously published study (Sharma et al., 2019).

2.3. Data preprocessing

Data were preprocessed using statistical parametric mapping (SPM12) and JIP software (https://www.nitrc.org/projects/jip). Data were corrected for motion-related artefacts by spatially realigning all the functional images to the first image of the first run. Rigid and non-rigid co-registration of these realigned images to a template anatomy (monkey M12; Ekstrom et al., 2008; Nelissen and Vanduffel, 2011) was then performed using JIP. Consequently, these coregistered images were resliced to 1 mm isotropic voxel size and smoothed with a 2.5 mm Gaussian kernel.

2.4. Hierarchical clustering

After preprocessing, the data were bandpass filtered between 0.0025 and 0.05 Hz (Mantini et al., 2011; Vincent et al., 2007). Following bandpass filtering, hierarchical clustering analysis was performed on the data using the standard functions associated with this method in MATLAB ('pdist' and 'linkage'). This method for the hierarchical clustering has been previously described in Hutchison and Everling (2014) and Schaeffer et al. (2019a, 2019b) and thus will only be reviewed here briefly.

Since we were interested in examining the organization of the ventral premotor cortex F5 and neighboring area 44, we restricted the clustering analysis to a mask (defined on the left hemisphere template anatomy) including the fundus and the posterior bank of the lower arcuate sulcus, along with the adjacent cortical convexity (Fig. 1A, red). The extent of this mask was guided by structural landmarks and based on previous anatomical and functional studies as specified below. In the posterior bank of the arcuate sulcus and the adjacent convexity, the mask included all three sub-divisions of premotor F5 - F5a, F5p and F5c

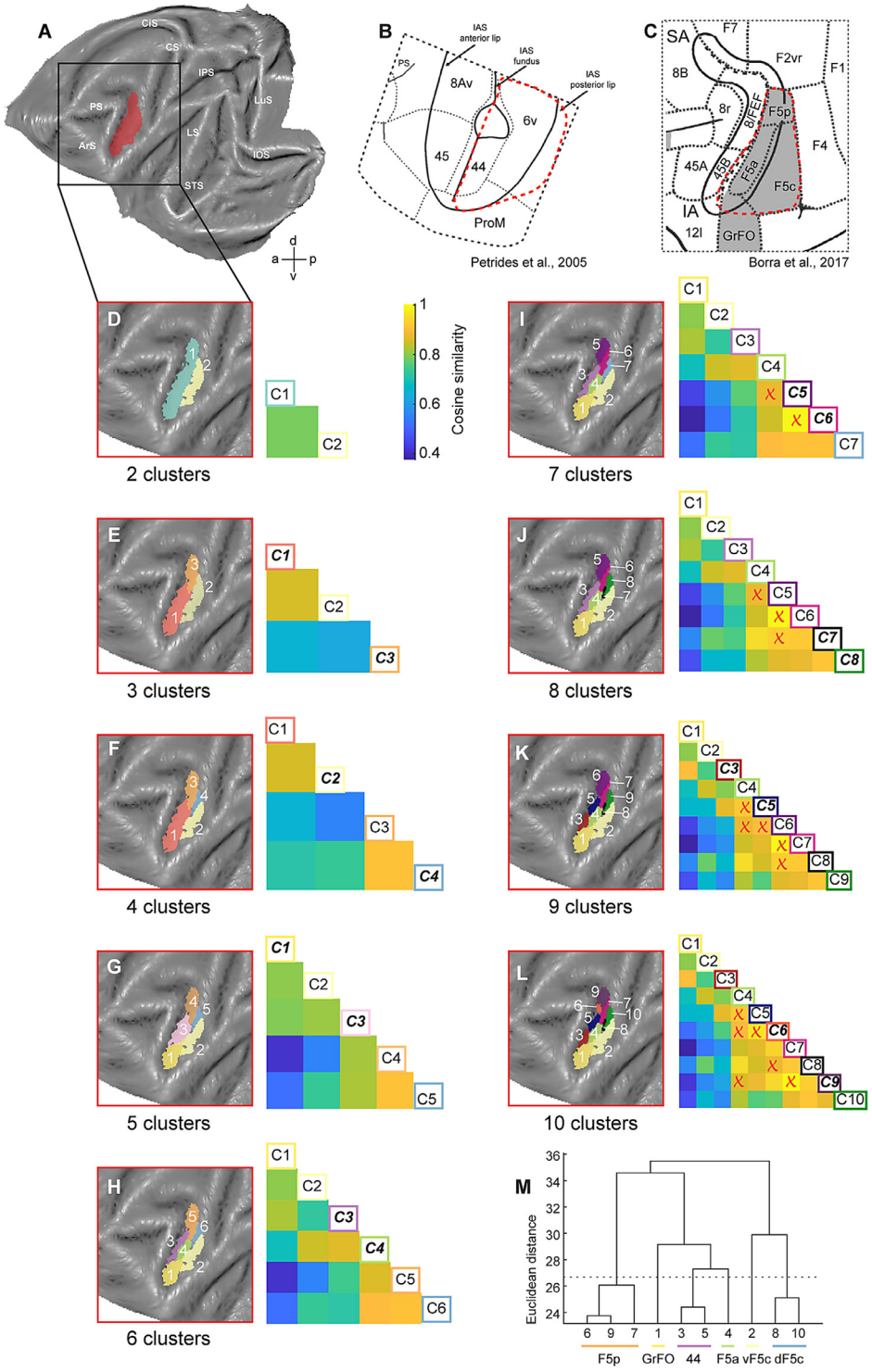

Fig. 1. Hierarchical clustering analysis of the inferior arcuate sulcus in the left hemisphere. **A.** The full mask (red) used in the clustering analysis included the fundus and posterior bank of inferior arcuate sulcus and adjacent post-arcuate convexity. **B, C.** Two parcellation schemes for the lower arcuate and adjacent convexity as in (**B**) Petrides et al. (2005) (adapted with permission from Belmalih et al., 2009) and (**C**) Borra et al. (2017) (adapted with permission from Borra et al., 2017). **D-L.** Results of the hierarchical clustering analysis displaying the two through ten cluster solutions. The different colors indicate separate clusters for each cluster solution. The cosine similarity matrix adjacent to each cluster solution demonstrates the results of the pairwise comparison of each cluster with every other cluster within a cluster solution in terms of their interareal functional connectivity (or their 'fingerprint') with 19 external seeds (location of the 19 external seeds are demonstrated in Fig. S2B). The lower bound of the color bar corresponds to the lowest observed cosine similarity value of all two to ten solution cluster comparisons. Lower cosine similarity values indicate that the clusters demonstrate distinct functional connectivity with the 19 external seeds (dissimilar fingerprints) while higher cosine similarity values indicate similar functional connectivity of the clusters with the 19 external seeds (similar fingerprints). The square boxes around the cluster labels in the matrix are color-matched to the clusters demonstrated in the adjacent flat map. Bold cluster labels correspond to the new subclusters that emerge in each cluster solution (for example, C1 and C3 in the 3 cluster solution). Red crosses indicate the clusters that did not demonstrate significantly different fingerprints ($p<0.05$) measured by a permutation testing approach (see methods). Results of the permutation testing approach demonstrate that each cluster is distinct from every other cluster up until the 6-cluster solution in terms of their interareal connectivity, which supports the selection of six as the optimal number of clusters. **M.** A dendrogram of the ten-cluster solution. The cluster numbers on the x-axis correspond to the numbers of the 10-cluster solution displayed on a flat map in (**L**). The six regions underneath the x-axis display the correspondence of cluster numbers from the ten-cluster solution to the regions of the six-cluster solution, which was selected as the optimal cluster solution. For instance, cluster 6, 9 and 7 in the 10-cluster solution are the sub-clusters of the original F5p cluster from the 6-cluster solution. a: anterior, p: posterior, d: dorsal, v: ventral. (For interpretation of the references to colour in this figure legend, the reader is referred to the web version of this article.)

(Nelissen et al., 2005, 2018; Belmalih et al., 2009; Maranesi et al., 2012). Furthermore, the mask extended deep into the fundus of the arcuate sulcus where dysgranular area 44 has been described (Petrides et al., 2005; Belmalih et al., 2009; Frey et al., 2014; Neubert et al., 2014; Caminiti et al., 2017; Palomero-Gallagher and Zilles, 2018). Finally, the mask extended slightly further ventral from areas 44 and F5a, thus, possibly including a portion of area GrFO (Belmalih et al., 2009; Gerbella et al., 2016, 2011) in the most antero-ventral part of the fundus. This was done to ensure that the entire posterior bank and the fundus of the arcuate were included in the mask, since the precise extent and location of F5a, area 44 and the portion of GrFO in the fundus and bank of the lower arcuate are difficult to define precisely without more invasive investigations. A similar mask was also delineated in the right hemisphere, in order to assess the reliability of the cluster solutions across both hemispheres (Hutchison and Everling, 2014; Schaeffer et al., 2019a).

Once the mask in the arcuate sulcus and adjacent convexity had been delineated, the time courses for each voxel within this mask were extracted for each run. These time courses were then used to calculate the partial correlation of each voxel with every other voxel within the

mask, using the three dimensional motion parameters and their first derivatives, mean white matter and ventricles time courses as nuisance regressors. The obtained correlation values were Fischer transformed to z-scores, which were averaged across runs within monkeys and then across monkeys to give an average pairwise z-score matrix of all the voxels within the mask. This average z-score matrix was subsequently converted to a distance matrix by computing the pairwise standard Euclidean distance between all the voxels (using the 'pdist' function in MATLAB), in order to obtain the voxel to voxel dissimilarity of their temporal correlations. Finally, the resulting Euclidean distance matrix was subjected to unweighted average-linkage hierarchical clustering analysis to delineate the functional cluster solutions within the arcuate sulcus mask. The functional clusters obtained from this analysis were projected on flattened representations of our macaque anatomical template (M12 of Ekstrom et al., 2008) using Caret software (version 5.65) for display purposes. For supplementary figure S1, the clusters were also displayed on coronal sections of the anatomical template using the software FSLeyes (https://fsl.fmrib.ox.ac.uk/fsl/fslwiki/FSLeyes). The clusters within each cluster solution were consequently subjected to a permutation testing approach (detailed below) in order to select the optimal cluster solution. Finally, the clusters from the optimal cluster solution were used as seeds to conduct a seed-to-brain functional connectivity analysis.

2.5. Fingerprinting and permutation testing

To test if the clusters were significantly different to each other in terms of their extrinsic interareal connectivity (or their 'fingerprints', Mars et al., 2016), we employed a permutation testing approach similar to Schaeffer et al. (2020). In order to do the fingerprinting, we first selected 19 different spheres of 2 mm radius as seeds located in/near functionally responsive hand/mouth related regions (10 hand related and 9 mouth related) external to the hierarchical clustering mask, which were the same seeds as used in our previous seed-to-brain resting-state study (Sharma et al., 2019). Hand-related regions/seeds include the medial portion of primary motor cortex (F1), primary somatosensory cortex (S1) and secondary somatosensory cortex (S2) in addition to the dorsal portion of the caudal sector of the ventral premotor cortex (dorsal F4), four parietal regions - PE, PEip, AIP, PFG and finally, posterior insula. Mouth-related regions/seeds include the lateral portion of the F1, S1 and S2, the ventral part of F4, PF in the parietal cortex, anterior insula, primary gustatory cortex in the operculum adjacent to anterior insula, and three regions in the frontal operculum – DO, PrCO and GrFO (convexity). We then conducted a seed-to-seed correlation analysis per run by correlating the mean time course of each cluster (average of all the voxels within a cluster) to the mean time course of each of the 19 seed regions, after bandpass filtering the data and parsing out white matter, ventricles and motion regressors. This resulted in a 19 x n correlation matrix per run, where n is the number of clusters, which was converted to a z-score matrix by Fisher's r-to-z transformation, and then averaged across runs per monkey. Each column in the average z-score matrix per monkey, which contains the correlation of a cluster with the 19 external seeds, is referred to as the 'fingerprint' of the cluster (Mars et al., 2016; Schaeffer et al., 2020) and we obtained a fingerprint for each cluster that emerged in the 2 to 10 cluster solutions. The fingerprints were then normalized to a range between 0 and 1, and pairwise comparison between clusters was performed by calculating the cosine similarity between the normalized fingerprints of the clusters. Cosine similarity is a scale invariant similarity measure and takes values from −1 for opposed fingerprints to 1 for identical fingerprints. To test for statistical differences between each pair of cluster fingerprints, a permutation test at the subject level was performed using an in-house code written in Matlab. First, the two cluster labels for a given pair were randomly shuffled per monkey, followed by averaging the fingerprints across monkeys (separately for each cluster label), normalizing the average fingerprints between 0 and 1, and calculating the cosine similarity between the normalized fingerprints. This process was iterated 100,000 times, to estimate a distribution of cosine similarities under the null hypothesis that the two clusters have the same fingerprint. A p-value <0.05 (i.e. >95% of the permutation values of cosine similarity were larger than the observed value) was taken to indicate significantly different fingerprints (Exact p-values for all cluster comparisons are reported in Table S1-S9).

2.6. Seed-based functional connectivity analysis

After conducting bandpass filtering of the data (0.0025–0.05 Hz) and regression of white matter, ventricles and motion parameters, the mean representative time course was obtained by averaging the signal across all the voxels within the functional clusters (Mantini et al., 2011; Sharma et al., 2019; Vincent et al., 2007). Whole-brain connectivity maps were created by calculating the correlations between the signals in the clusters and each voxel in the rest of the brain. Individual whole-brain connectivity maps were converted to z scores by Fisher's *r*-to-*z* transformation. A fixed-effect analysis was used to create group-level correlation maps (Mantini et al., 2011; Touroutoglou et al., 2016), which were thresholded at $z > 2.3$ or $z > 3.1$ (Ghahremani et al., 2016; Hutchison et al., 2015, 2012a; Sharma et al., 2019). These group-level z-score maps were projected on flattened representations of M12 anatomical template using Caret software (version 5.65).

3. Results

3.1. Hierarchical clustering of the arcuate sulcus

In this study, we performed hierarchical clustering analysis on the voxels within a mask that extended from the fundus and posterior bank of the lower arcuate sulcus to the adjacent cortical convexity (Fig. 1A, mask in red). According to the architectonic parcellation scheme suggested by Petrides et al. (2005), our mask included area 44 in the fundus, part of ProM in the antero-ventral tip of the fundus and lower arcuate, in addition to area 6v in the posterior bank and adjacent convexity (red outline in Fig.1B). According to the parcellation schemes suggested by Luppino and co-authors (Borra and Luppino, 2017; Caminiti et al., 2017; see also Belmalih et al., 2009), our mask included the 3 subdivisions of area F5 (F5c, F5p and F5a), the fundus between F5a and prefrontal 45B (unlabeled in Borra and Luppino, 2017 but referred to as area 44 in the parcellation scheme by Belmalih and co-authors, see Fig. 1 in Belmalih et al., 2009), and part of area GrFO in the anterior end of the lower arcuate (part of ProM according to Petrides et al., 2005) (red outline in Fig. 1C). Hierarchical clustering does not require a specification of the maximum number of clusters and is only limited by the number of data points being clustered (Hutchison and Everling, 2014). However, since our aim was exploratory, we conducted the analysis for two through ten cluster solutions.

Fig. 1D-L shows the result of the hierarchical clustering analysis for two to ten cluster solutions in the left hemisphere. Without any a priori knowledge, it is difficult to assess the overall optimal number of clusters that would be most representative of the underlying functional/anatomical specialization. One way to address this issue, while being independent of a priori assumptions based on previous parcellation schemes, is to select a cluster solution as optimal, beyond which a cluster and subsequent sub-clusters stop differentiating in terms of their extrinsic interareal connectivity (Schaeffer et al., 2020). To do this, we first selected 19 seeds from different regions in the brain located outside of the mask we used for the hierarchical clustering analysis (Fig. S2B). These seeds corresponded to brain regions associated with hand and mouth movements, as demonstrated by both resting-state and task-based fMRI (Sharma et al., 2019). We then computed the correlation of each cluster within a cluster solution with the 19 external seeds, referred to as their 'fingerprints' (Mars et al., 2016; Schaeffer et al., 2020), which were consequently converted to z-scores using the Fisher's r to z transformation. Similarity of cluster fingerprints was measured using a

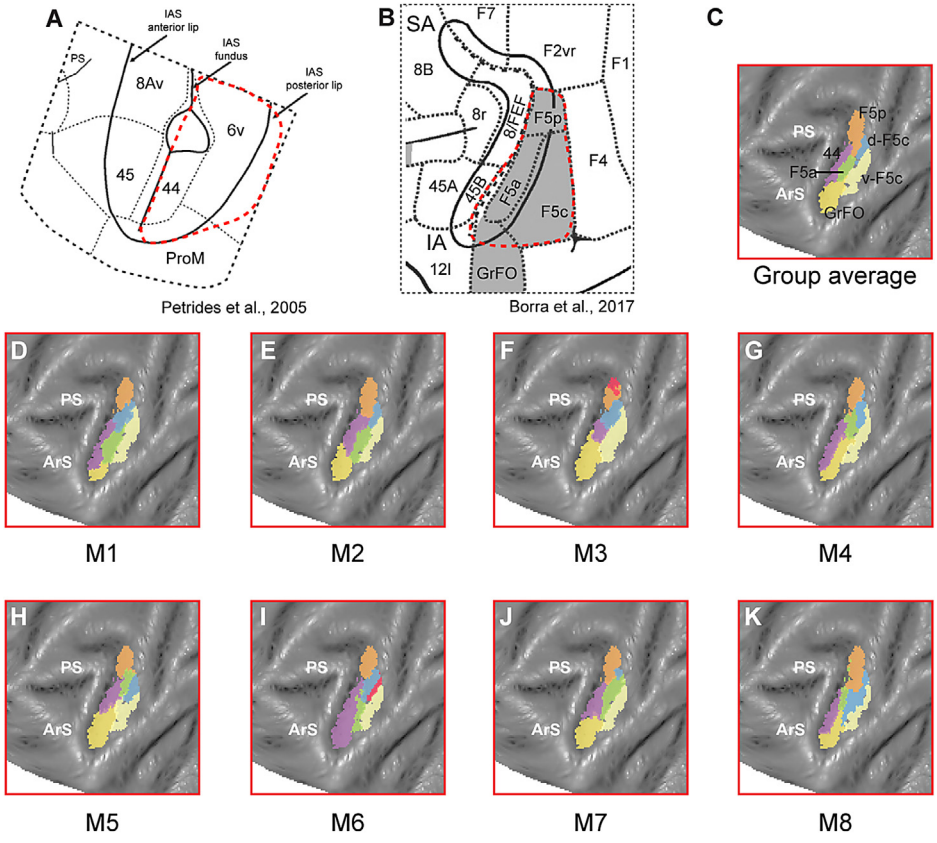

Fig. 2. Hierarchical clustering analysis of the inferior arcuate sulcus at the single subject level. **A, B.** Two parcellation schemes for the lower arcuate and adjacent convexity as in (**A**) Petrides et al. (2005) (adapted with permission from Belmalih et al., 2009) and (**B**) Borra et al. (2017) (adapted with permission from Borra et al., 2017). **C.** The six cluster solution of the group average which was selected as the optimal cluster solution on the basis of permutation testing approach. **D-K.** The six cluster solution that resulted from conducting hierarchical clustering analysis for the each of the eight monkeys individually. The colors of the clusters for each monkey were denoted according to the relative correspondence of the cluster with the regions suggested in the group average (F5p: orange, D-F5c: blue, v-F5c: light yellow, F5a: green, area 44: purple and GrFO: mustard). Clusters that could not be classified as any of these regions are shown in red. (For interpretation of the references to colour in this figure legend, the reader is referred to the web version of this article.)

cosine similarity index, normalized to a range between zero and one, with values closer to zero indicating dissimilar fingerprints and values closer to one indicating similar fingerprints. The cosine similarity matrix adjacent to each flatmap in Fig. 1D-L demonstrates the cosine similarity values for the pairwise comparisons of all the clusters within a cluster solution. We employed a permutation testing approach (see Methods; Schaeffer et al., 2020) to examine if the clusters within each cluster solution were significantly different ($p<0.05$) from each other in terms of their fingerprints (red crosses in the cosine similarity matrices indicate clusters that did not demonstrate significantly different fingerprints ($p<0.05$) measured by a permutation testing approach) for each cluster solution in Fig. 1D-L. Corresponding p-values for each cluster solution are listed in Tables S1-S9). Permutation testing demonstrated that up until the six cluster solution, each cluster is significantly different from every other cluster ($p<0.05$) within the cluster solution in terms of their extrinsic interareal connectivity or their fingerprint (Fig. 1D-H). For the seven cluster solution, the sub-clusters that emerge (cluster 5 and cluster 6; Fig. 1I) are not significantly different from each other in terms of their fingerprints (Fig. 1I, cosine similarity = 0.99, $p = 0.54$, Table S5). Additionally, cluster 4 and cluster 5 in the seven cluster solution are also not significantly different from each other (cosine similarity = 0.88, $p = 0.087$, Table S5). Similarly, the sub-clusters emerging in the eight cluster solution and beyond do not seem to demonstrate statistically different fingerprints (Fig. 1J-L, Table S7-S9). Thus, this approach would suggest that the six clusters are the optimal number of clusters since the clusters within the six cluster solution are significantly different from each other in terms of their extrinsic interareal connectivity, beyond which this cluster dissimilarity seems to break down.

Next, having established the six-cluster solution as optimal, we examined how it compares to the previously suggested partitioning schemes derived from invasive functional and anatomical investigations. In reference to these partitioning schemes (Fig. 1B, C), the dorso-posterior cluster (orange in Fig. 1H) corresponds to the location suggested for F5p in the posterior bank of the arcuate (Nelissen et al., 2005; Belmalih et al., 2009; Borra et al., 2017; Fig. 1C). The two clusters on the convexity of the arcuate seem to correspond F5c, with a smaller dorsal (Fig. 1H, blue) and a larger ventral cluster (Fig. 1H, light yellow), which appears to reflect the dorsal to ventral functional specialization suggested for this region with respect to hand- and mouth actions (Ferrari et al., 2017; Sharma et al., 2019). The location of the two clusters anterior to F5c seem to correspond with the suggested location of area F5a on the posterior bank (green in Fig. 1H) and area 44 in the fundus (purple in Fig. 1H) of the lower arcuate (Belmalih et al., 2009; Borra and Luppino, 2017; Petrides et al., 2005). Finally, the most anterior cluster in the tip of the fundus and lower bank of the arcuate (mustard in Fig. 1H) possibly corresponds to a part of ProM (in Petrides et al., 2005; Fig. 1B) or GrFO (according to Gerbella et al., 2016; Borra and Luppino, 2017; Fig1C). For the seven to ten cluster solutions, several additional small clusters appeared (seven clusters, Fig. 1I: breakdown of F5p, eight clusters, Fig. 1J: breakdown of dorsal F5c, nine clusters, Fig. 1K: breakdown of 44, ten clusters, Fig. 1L: further breakdown of F5p), for which a direct correspondence to currently known functional/anatomical organizations of the lower arcuate is not straightforward.

In order to examine the reliability of the six cluster solution at the single subject level, we also conducted hierarchical clustering analysis for each of the eight monkeys individually (Fig. 2D-K). It is evident that, though the relative size of the clusters across monkeys is variable, in at least 6 out of 8 monkeys the six cluster solution shows good correspondence with the group average (Fig. 1H, Fig. 2C) and the suggested parcellation schemes based on invasive evidence (Fig. 2A,B; Petrides et al., 2005; Borra et al., 2017; Ferrari et al., 2017).

Finally, in order to investigate reliability of the six cluster solution across hemispheres, we conducted a similar hierarchical clustering analysis for the right hemisphere independently from the left hemisphere. Fig. S1 shows the six cluster solution in the right hemisphere on a

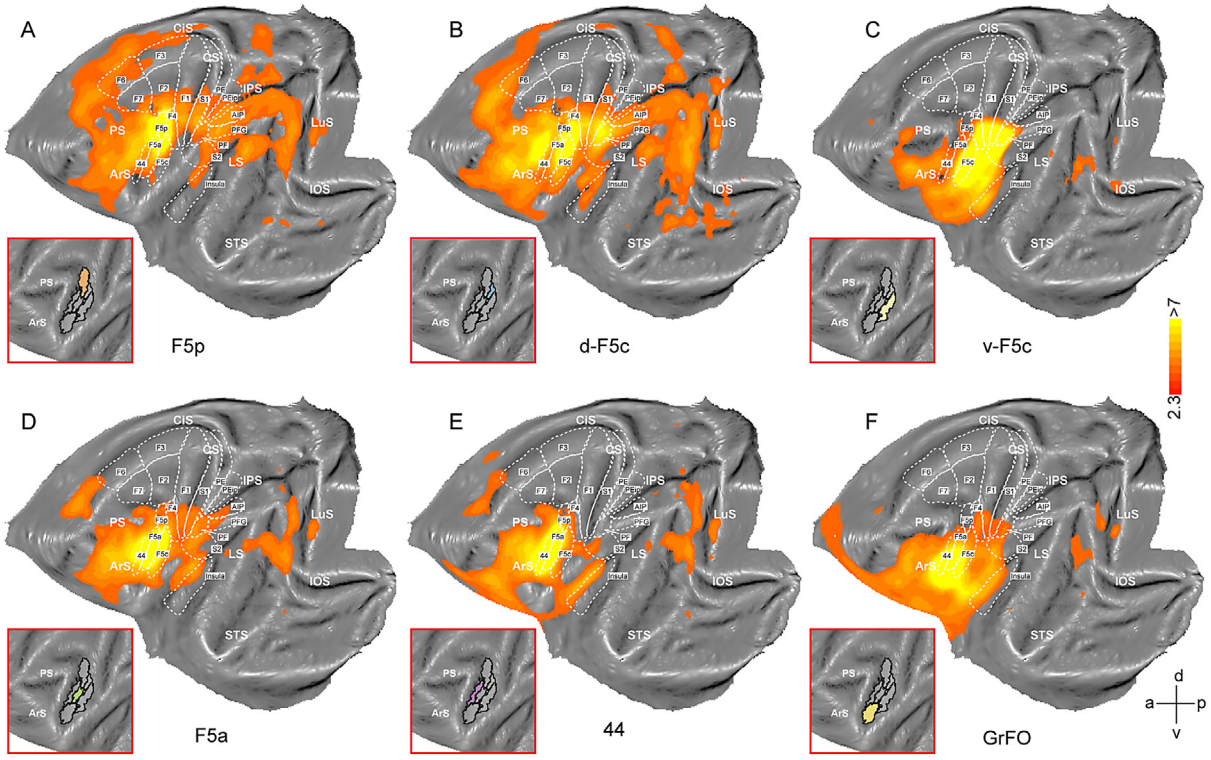

Fig. 3. Seed-based functional connectivity of the six clusters in the left hemisphere. **A-F**. Whole brain functional connectivity of clusters corresponding to F5p (**A**), dorsal F5c (**B**), ventral F5c (**C**), F5a (**D**), area 44 (**E**), and (part of) GrFO (**F**). Insets indicate the location of the cluster that was used as a seed for the whole brain correlation maps. a: anterior, p: posterior, d: dorsal, v: ventral.

flatmap (Fig. S1A) and sections (Fig. S1B). Similar to the left hemisphere, the six-cluster solution in the right hemisphere also shows a high correspondence with the suggested parcellation scheme of this region, with a cluster corresponding to the location of F5a (Fig. S1A, B, green) and F5p (Fig. S1A, B, orange) at different antero-posterior position on the posterior bank of the arcuate, dorsal and ventral portions of F5c on the convexity (Fig. S1A, B, blue and light yellow), area 44 in the fundus of the arcuate anterior to F5a (Fig. S1A, B, purple), and part of ProM or GrFO in the anterior tip of the bank and fundus of the lower arcuate (Fig. S1A, B, mustard).

3.2. Seed-based correlation analysis of the F5/44/GrFO clusters

Aside from comparing the anatomical location of the distinct clusters with partitioning schemes derived from invasive functional or architectonical investigations, we also investigated the functional connectivity of each of these clusters with the rest of the brain, in an attempt to examine the possible correspondence of these clusters with previously described connectivity of different anatomical/functional sub-regions in the lower arcuate. Therefore, we performed a voxel-wise seed-to-brain connectivity analysis with the clusters obtained from the six cluster solution. This allowed us to assess how functional connectivity of these clusters resembled previous invasive tract tracing and seed-based resting-state studies, describing the connectivity of the different functional subfields in the inferior arcuate of the macaque monkey (Frey et al., 2014; Gerbella et al., 2016, 2011; Neubert et al., 2014; Sharma et al., 2019).

In the posterior bank of the arcuate sulcus, the six cluster solution of the hierarchical clustering analysis resulted in a cluster in the most dorsal portion of the posterior bank of the lower arcuate, which based upon its location corresponds to F5p (orange in Fig. 1H and in inset in Fig. 3A). This cluster showed functional correlations across prefrontal cortex, including 45, 46 and FEF, in addition to premotor areas F5a, area 44, dorsal parts of F5c, F4, primary motor cortex F1, primary somatosensory cortex S1, as well as portions of cingulate cortex and dorsal premotor areas F2, F3, F6, F7, posterior part of S2 and insula, superior and inferior parietal cortex and posterior STS (Fig. 3A). On the postarcuate convexity, two clusters (blue and light yellow in Fig. 1H and insets in Fig. 3B,C) were observed in the six cluster solution. Their location and functional connectivity correspond to those described for the dorsal (hand-dominated) and ventral (mouth-dominated) portions of premotor F5c (Ferrari et al., 2017; Sharma et al., 2019). The most dorsal of these two clusters (inset Fig. 3B, blue) showed functional correlations with all other parts of F5, 44, prefrontal cortex, parts of cingulate cortex and dorsal premotor areas F2, F6 and F7, area F4, area F1, portion of S1, S2, insula, parietal cortex, STS and extrastriate cortex. In contrast, the ventral cluster (inset Fig. 3C, light yellow) showed much more restricted functional correlations, in particular with ventral primary motor (F1) and somatosensory (S1) cortex, parietal area PF, prefrontal and orbitofrontal cortex, anterior S2 and insula, primary gustatory cortex and additional frontal opercular regions. Antero-ventral to the cluster we attributed to F5p on the posterior bank of the lower arcuate sulcus (Fig. 3A), another cluster was found (Fig. 1H). This cluster (inset Fig. 3D, green) showed functional correlations with the neighbouring premotor areas, in addition to area 44 and prefrontal areas, anterior cingulate, frontal opercular regions, posterior insula, ventral part of primary motor and somatosensory cortex, S2, parietal areas PF, PFG and AIP, and portion of early visual and STS. Both its connectivity profile and location suggest this cluster corresponds to F5a in the posterior bank of the lower arcuate. A fifth cluster (inset Fig. 3E, purple), located in the fundus of the arcuate, showed correlations with the subfields of premotor F5, in addition to prefrontal, orbitofrontal, cingulate and frontal opercular areas, a portion of S2, dorsal insula and early visual and STS. The location of this cluster corresponds with the location of area 44 as described by Petrides et al., 2005 and Belmalih et al., 2009. Finally, the sixth cluster located in the anterior ventral part of the fundus of the arcuate (Fig. 1H, inset Fig. 3F, mustard), showed correlations with the other subfields of premotor F5, area 44, prefrontal, orbitofrontal and frontal opercular, part of S2, and restricted portions of early visual areas and STS. Unlike

area 44, this cluster also showed functional correlations with ventral portions of F4, F1, S1 and PF in the parietal cortex. Based upon its location and functional connectivity profile, this cluster might correspond to a part of area GrFO (Belmalih et al., 2009; Gerbella et al., 2016; Sharma et al., 2019). Note that since our mask did not extend to the frontal operculum ventral to the inferior arcuate, our 'GrFO' cluster only included a part of GrFO as suggested by previous invasive investigations (Gerbella et al., 2016, 2011) and therefore the functional connectivity profile of our GrFO cluster is only representative for this dorsal portion of the GrFO region. Fig. S1C-–-H shows the whole brain functional connectivity maps of the six clusters for the right hemisphere, which shows overall good correspondence with the corresponding six clusters in the left hemisphere (Fig. 3A-F).

Finally, functional connectivity of the six clusters delineated by hierarchical clustering analysis showed high similarity to the functional connectivity of previous seed-based resting-state investigations using anatomical criteria to delineate the different arcuate regions (Neubert et al., 2014; see Fig. 2 and Fig. 3 of Sharma et al., 2019). The locations of the six clusters delineated in the current resting-state clustering study (Fig. S2A, colored regions) showed a great degree of overlap with the location of the seeds from a previous seed-based resting-state investigation (Sharma et al., 2019) that examined functional connectivity of seeds placed in the inferior arcuate and which locations were based upon anatomical and functional criteria (Fig. S2A, colored circles).

4. Discussion

Previous studies in primates have shown the promising application of using non-invasive resting-state fMRI data to map several organizational principles of different portions of the cortex (Goulas et al., 2017; Hutchison et al., 2012b; Hutchison and Everling, 2014; Schaeffer et al., 2019a, 2019b; Vijayakumar et al., 2018). In this study, we examined to what extent partitioning schemes of macaque inferior arcuate sulcus derived from data-driven hierarchical clustering analysis of resting-state fMRI data correspond to organizational schemes based upon functional/anatomical investigations. In particular, a six cluster solution resembled a level of organization that matches well with the organization of this portion of cortex as suggested by previous combined invasive architectonic and functional examinations. Permutation testing suggested that fingerprint connectivity of the clusters was significantly different for the six cluster solution. We attributed these six clusters to respectively the dorsal and ventral subdivisions of F5c on the postarcuate convexity, F5p and F5a on the posterior bank of the lower arcuate, area 44 in the fundus of the lower arcuate, and (part of) GrFO in the most antero-ventral portion of the fundus and posterior inferior arcuate.

4.1. Organization of macaque inferior posterior arcuate sulcus as suggested by functional, architectonic and connectional evidence

Ventral premotor cortex F5, occupying the posterior bank of the lower arcuate and adjacent convexity, originally considered to be one region (Matelli et al., 1985), was later demonstrated to be formed by two cytoarchitectonic subfields – F5ab on the posterior bank of the arcuate sulcus and F5c on the adjacent cortical convexity (Matelli et al., 1996). Later investigations suggested F5ab on the bank of the arcuate sulcus to consist of two distinct cytoarchitectonic subfields - F5a and F5p located on the posterior bank of the arcuate sulcus at different anterior-posterior positions (Nelissen et al., 2005; Belmalih et al., 2009). Electrophysiological and neuroimaging investigations of F5p have demonstrated that this region contains neurons that respond during skilled manual movements such as grasping or manipulating objects (Rizzolatti et al., 1988; Nelissen and Vanduffel, 2011; Nelissen et al., 2018). In agreement with this proposed functional specialization of F5p and tract-tracing evidence, the 'F5p' cluster in our study showed connections with other regions associated with hand/arm-related motor functions such as parietal areas PFG and AIP, dorsal premotor areas F2, F3, F6 and F7, and dorsal portions of F4 and F1. With regard to F5c, on the cortical convexity, functional and connectional evidence suggest that F5c contains a ventral portion that has been shown to be associated with mouth movements such as biting, chewing or lipsmacking and a dorsal portion that contains a hand and mouth representation (Ferrari et al., 2017, 2003; Gentilucci et al., 1988; Maranesi et al., 2012). In line with these observations, the cortical convexity posterior to the arcuate broke down into a dorsal ('dorsal F5c') and ventral part ('ventral F5c'), in our six cluster solution. Their functional connectivity maps supported the distinctness of the two clusters with the ventral F5c cluster having strong correlations with regions such as GrFO, PrCO and DO, ventral parts of F4, F1, and inferior parietal area PF, all of which are associated with mouth movements. The dorsal F5c cluster, on the other hand, showed overlapping connections with both hand and mouth movement associated regions which fits well with the proposed functional specialization of this region (Ferrari et al., 2017; Maranesi et al., 2012).

In line with previous cytoarchitectonic evidence (Belmalih et al., 2009; Nelissen et al., 2005), clustering also retrieved a cluster in the posterior bank of the arcuate sulcus anterior to F5p, corresponding to F5a. Anterior to the F5a cluster, an additional cluster located in the fundus of the lower arcuate was found, corresponding to the suggested location of area 44 (Belmalih et al., 2009; Petrides et al., 2005). Tract-tracing injections in F5a have demonstrated that it has connections with other hand-related regions such as AIP and PFG, in addition to mouth related regions such as GrFO and PrCO, which is also reflected in the whole brain connectivity maps of our F5a cluster (Fig. 3D). Functional investigations confirm the role of F5a in the visual analysis of 3-dimensional object properties related to object grasping (Joly et al., 2009; Theys et al., 2012). A specific role in grasping has so far not been described for area 44 in the fundus. This region seems to be involved in coding different aspects of mouth movements and responses have been described during communicative face movements including lip smacking (Petrides et al., 2005; Shepherd and Freiwald, 2018) or vocalizations (Hage and Nieder, 2013). While adjacent 'F5a' and '44′ clusters yielded substantial overlap in terms of their seed-to-brain functional correlations maps (Fig. 3D,E), both clusters also showed functional connectivity differences (in particular with respect to anterior parietal regions). Finally, the six cluster solution also showed a cluster in the ventral portion of the fundus of the inferior arcuate, which possibly corresponds to the dorsal part of area GrFO, which ventrally extends onto the frontal operculum (Gerbella et al., 2016, 2011). This 'GrFO' cluster demonstrated connections with F5a, 44, ventral F5c, DO, PrCO, insula and prefrontal and orbitofrontal cortices, in line with anatomical tract-tracing injections in this region (Ferrari et al., 2017; Gerbella et al., 2016). It will be interesting for future studies to quantitatively assess the correspondence of resting-state fMRI derived clusters with the anatomo-functional regions delineated by more invasive procedures in the same animals, particularly in view of the individual variability observed in the relative size of the clusters (Fig. 2D-K). Although we considered in this study the 6 cluster partitioning scheme as the optimal number of clusters based upon the fingerprinting/permutation method and the symmetry of this cluster solution found in both hemispheres, it is possible that higher cluster numbers might represent true connectional/functional differences that still need to be established with more invasive methods.

It should be noted that functional connectivity as measured by resting-state fMRI has some discrepancies with connection profiles demonstrated through tract-tracing injections and may not reflect direct anatomical connections (Howells et al., 2020). For instance, the F5 clusters in our current study show functional connectivity with parts of early visual areas and the posterior part of STS, which do not seem to reflect known anatomical connections. Though injections in F5a or 44 have been associated with labeling in parts of the STS (Frey et al., 2014; Gerbella et al., 2011), the functional connectivity between the other sub-sectors of F5 and posterior STS in our data might be reflective of polysynaptic connections (Honey et al., 2009; Hutchison and Everling, 2014; Vincent et al., 2007).

4.2. Organization of macaque inferior posterior arcuate sulcus as suggested by previous resting-state fMRI investigations

Several authors have used data-driven clustering analyses to examine the organization of the macaque frontal cortex, including the arcuate region. For instance, Hutchison and Everling (2014) employed hierarchical clustering analysis on the frontal cortex, and found the five cluster solution to be optimal in their study. Their broad "caudal cluster" overlaps with the location of area F5p on the posterior bank of the arcuate sulcus, but also extends rostrally until the principal sulcus, thus presumably including areas 8Ad and 8Av, 9/46d, parts of 9/46v, and parts of area 8B, and area 46 (Petrides and Pandya, 2002). Furthermore, their "lateral cluster" included most of the cortex around the lower limb of the arcuate sulcus, extending both rostrally and caudally on the convexity, thus including areas 45A, 45B, and parts of 47/12 and 9/46 along with areas 44, F5a and F5c.

Clustering within a large frontal cortex mask, Goulas et al. (2017) found nineteen to be an optimal cluster solution for their investigation. They reported a cluster labeled as area 44 in the fundus of the arcuate separate from another cluster located on the ventral convexity and referred to as F5c. As both their 44 and F5c clusters appear to extend slightly onto the anterior bank of the arcuate sulcus, F5a is likely to be included in one (or both) of these clusters. Moreover, Goulas et al. (2017) did not describe a separate cluster corresponding to area F5p in their study, although they acknowledged that their FEF/8Av cluster (dorsal to the area 44 cluster) possibly included part of ventral premotor cortex, since it included the posterior bank of the arcuate sulcus. Finally, using a twenty-six cluster solution, Vijayakumar and colleagues (2018) described a cluster they referred to as area 8, which possibly includes both F5p and FEF. Additionally, they described an area F5 on the ventral postarcuate convexity, which possibly corresponds to a part of F5c. However, this F5 cluster extends laterally onto the frontal operculum and therefore possibly also includes (part of) areas GrFO, PrCO and DO (Gerbella et al., 2016). Anterior to this cluster, they described an area 44 cluster, which seems to include F5a on the posterior bank as well.

A distinction between previous data-driven resting-state investigations and our current study is the extent of the mask on which the clustering analysis was conducted. These aforementioned macaque resting-state studies used a larger mask including prefrontal cortex and the arcuate (Hutchison and Everling, 2014), or the entire frontal cortex extending rostrally from the central sulcus (Goulas et al., 2017; Vijayakumar et al., 2018). In contrast, our mask in the current study was much more restricted and included only the inferior arcuate fundus, posterior bank and adjacent convexity. Possibly some of the described larger clusters in/near the arcuate sulcus in these previous macaque resting-state studies might still breakdown into smaller clusters, resembling our current findings. Depending on the specific scientific question(s) at hand, the extent of the mask and the optimal number of clusters will most likely differ between studies (Schaeffer et al., 2019a).

Although the exact correspondence between resting-state derived clusters and underlying architectonical/functional organization as demonstrated from more invasive evidence still needs further investigations and might vary depending on the cortical region (Schaeffer et al., 2019a), our current study suggests that hierarchical clustering analysis of resting-state fMRI data can retrieve a fine-grained level of cortical organization that resembles detailed parcellation schemes derived from invasive functional and anatomical investigations.

Acknowledgements

We thank W. Depuydt, M. De Paep, C. Fransen, A. Hermans, P. Kayenbergh, G. Meulemans, I. Puttemans, C. Ulens and S. Verstraeten for technical assistance.

Funding

This work was supported by Fonds Wetenschappelijk Onderzoek Vlaanderen (G.0.622.08, G.0.593.09, G.0.854.19, V419419N) and KU Leuven (BOF-ZAP Start financing (14/10), C14/17/109).

Supplementary materials

Supplementary material associated with this article can be found, in the online version, at doi:10.1016/j.neuroimage.2020.117647.

References

Agcaoglu, O., Wilson, T.W., Wang, Y., Stephen, J., Calhoun, V.D., 2019. Resting state connectivity differences in eyes open versus eyes closed conditions. Hum. Brain Mapp. 40, 2488–2498. doi:10.1002/hbm.24539.

Belmalih, A., Borra, E., Contini, M., Gerbella, M., Rozzi, S., Luppino, G., 2009. Multimodal architectonic subdivision of the rostral part (area F5) of the macaque ventral premotor cortex. J. Comp. Neurol. 512, 183–217. doi:10.1002/cne.21892.

Borra, E., Gerbella, M., Rozzi, S., Luppino, G., 2017. The macaque lateral grasping network: a neural substrate for generating purposeful hand actions. Neurosci. Biobehav. Rev. 75, 65–90. doi:10.1016/j.neubiorev.2017.01.017.

Borra, E., Luppino, G., 2017. Functional anatomy of the macaque temporo-parieto-frontal connectivity. Cortex 97, 306–326. doi:10.1016/j.cortex.2016.12.007.

Caminiti, R., Borra, E., Visco-Comandini, F., Battaglia-Mayer, A., Averbeck, B.B., Luppino, G., 2017. Computational architecture of the Parieto-Frontal network underlying cognitive-motor control in monkeys. eNeuro 4. doi:10.1523/ENEURO.0306-16.2017, ENEURO.0306-16.2017.

di Pellegrino, G., Fadiga, L., Fogassi, L., Gallese, V., Rizzolatti, G., 1992. Understanding motor events: a neurophysiological study. Exp. Brain Res. 91, 176–180. doi:10.1007/BF00230027.

Ekstrom, L.B., Roelfsema, P.R., Arsenault, J.T., Bonmassar, G., Vanduffel, W., 2008. Bottom-up dependent gating of frontal signals in early visual cortex. Science (80-.). 321, 414–417. 10.1126/science.1153276

Ferrari, P.F., Gallese, V., Rizzolatti, G., Fogassi, L., 2003. Mirror neurons responding to the observation of ingestive and communicative mouth actions in the monkey ventral premotor cortex. Eur. J. Neurosci. 17, 1703–1714. doi:10.1046/j.1460-9568.2003.02601.x.

Ferrari, P.F., Gerbella, M., Coudé, G., Rozzi, S., 2017. Two different mirror neuron networks: the sensorimotor (hand) and limbic (face) pathways. Neuroscience 358, 300–315. doi:10.1016/j.neuroscience.2017.06.052.

Frey, S., Mackey, S., Petrides, M., 2014. Cortico-cortical connections of areas 44 and 45B in the macaque monkey. Brain Lang. 131, 36–55. doi:10.1016/j.bandl.2013.05.005.

Gentilucci, M., Fogassi, L., Luppino, G., Matelli, M., Camarda, R., Rizzolatti, G., 1988. Functional organization of inferior area 6 in the macaque monkey. Exp. brain Res. 71, 475–490.

Gerbella, M., Belmalih, A., Borra, E., Rozzi, S., Luppino, G., 2011. Cortical connections of the anterior (F5a) subdivision of the macaque ventral premotor area F5. Brain Struct. Funct. 216, 43–65. doi:10.1007/s00429-010-0293-6.

Gerbella, M., Borra, E., Rozzi, S., Luppino, G., 2016. Connections of the macaque Granular Frontal Opercular (GrFO) area: a possible neural substrate for the contribution of limbic inputs for controlling hand and face/mouth actions. Brain Struct. Funct. 221, 59–78. doi:10.1007/s00429-014-0892-8.

Ghahremani, M., Hutchison, R.M., Menon, R.S., Everling, S., 2016. Frontoparietal functional connectivity in the common marmoset. Cereb. Cortex 27, 3890–3905. doi:10.1093/cercor/bhw198.

Goulas, A., Stiers, P., Hutchison, R.M., Everling, S., Petrides, M., Margulies, D.S., 2017. Intrinsic functional architecture of the macaque dorsal and ventral lateral frontal cortex. J. Neurophysiol. 117, 1084–1099. doi:10.1152/jn.00486.2016.

Hage, S.R., Nieder, A., 2015. Audio-vocal interaction in single neurons of the monkey ventrolateral prefrontal cortex. J. Neurosci. 35, 7030–7040. doi:10.1523/JNEUROSCI.2371-14.2015.

Hage, S.R., Nieder, A., 2013. Single neurons in monkey prefrontal cortex encode volitional initiation of vocalizations. Nat. Commun. 4, 2409. doi:10.1038/ncomms3409.

Honey, C.J., Sporns, O., Cammoun, L., Gigandet, X., Thiran, J.P., Meuli, R., Hagmann, P., 2009. Predicting human resting-state functional connectivity from structural connectivity. Proc. Natl. Acad. Sci. 106, 2035–2040. doi:10.1073/pnas.0811168106.

Howells, H., Simone, L., Borra, E., Fornia, L., Cerri, G., Luppino, G., 2020. Reproducing macaque lateral grasping and oculomotor networks using resting state functional connectivity and diffusion tractography. Brain Struct. Funct. 225, 2533–2551. doi:10.1007/s00429-020-02142-2.

Hutchison, R.M., Culham, J.C., Flanagan, J.R., Everling, S., Gallivan, J.P., 2015. Functional subdivisions of medial parieto-occipital cortex in humans and nonhuman primates using resting-state fMRI. Neuroimage 116, 10–29. doi:10.1016/j.neuroimage.2015.04.068.

Hutchison, R.M., Everling, S., 2014. Broad intrinsic functional connectivity boundaries of the macaque prefrontal cortex. Neuroimage 88, 202–211. doi:10.1016/j.neuroimage.2013.11.024.

Hutchison, R.M., Gallivan, J.P., Culham, J.C., Gati, J.S., Menon, R.S., Everling, S., 2012a. Functional connectivity of the frontal eye fields in humans and macaque monkeys investigated with resting-state fMRI. J. Neurophysiol. 107, 2463–2474. doi:10.1152/jn.00891.2011.

Hutchison, R.M., Womelsdorf, T., Gati, J.S., Leung, L.S., Menon, R.S., Everling, S., 2012b. Resting-state connectivity identifies distinct functional networks in macaque cingulate cortex. Cereb. Cortex 22, 1294–1308. doi:10.1093/cercor/bhr181.

Joly, O., Vanduffel, W., Orban, G.A., 2009. The monkey ventral premotor cortex processes 3D shape from disparity. Neuroimage 47, 262–272. doi:10.1016/j.neuroimage.2009.04.043.

Kolster, H., Mandeville, J.B., Arsenault, J.T., Ekstrom, L.B., Wald, L.L., Vanduffel, W., 2009. Visual field map clusters in macaque extrastriate visual cortex. J. Neurosci. 29, 7031–7039. doi:10.1523/JNEUROSCI.0518-09.2009.

Mantini, D., Gerits, A., Nelissen, K., Durand, J.-.B., Joly, O., Simone, L., Sawamura, H., Wardak, C., Orban, G.A., Buckner, R.L., Vanduffel, W., 2011. Default mode of brain function in monkeys. J. Neurosci. 31, 12954–12962. doi:10.1523/JNEUROSCI.2318-11.2011.

Maranesi, M., Rodà, F., Bonini, L., Rozzi, S., Ferrari, P.F., Fogassi, L., Coudé, G., 2012. Anatomo-functional organization of the ventral primary motor and premotor cortex in the macaque monkey. Eur. J. Neurosci. 36, 3376–3387. doi:10.1111/j.1460-9568.2012.08252.x.

Mars, R.B., Verhagen, L., Gladwin, T.E., Neubert, F.-.X., Sallet, J., Rushworth, M.F.S., 2016. Comparing brains by matching connectivity profiles. Neurosci. Biobehav. Rev. 60, 90–97. doi:10.1016/j.neubiorev.2015.10.008.

Matelli, M., Luppino, G., Govoni, P., Geyer, S., 1996. Anatomical and Functional Subdivisions of Inferior Area 6 in Macaque Monkey 11858/00-001M-0000-0010-EDD0-B.

Matelli, M., Luppino, G., Rizzolatti, G., 1985. Patterns of cytochrome oxidase activity in the frontal agranular cortex of the macaque monkey. Behav. Brain Res. 18, 125–136. doi:10.1016/0166-4328(85)90068-3.

Murata, A., Fadiga, L., Fogassi, L., Gallese, V., Raos, V., Rizzolatti, G., 1997. Object representation in the ventral premotor cortex (Area F5) of the Monkey. J. Neurophysiol. 78, 2226–2230. doi:10.1152/jn.1997.78.4.2226.

Nelissen, K., Fiave, P.A., Vanduffel, W., 2018. Decoding grasping movements from the Parieto-frontal reaching circuit in the nonhuman primate. Cereb. Cortex 28, 1245–1259. doi:10.1093/cercor/bhx037.

Nelissen, K., Luppino, G., Vanduffel, W., Rizzolatti, G., Orban, G.A., 2005. Observing others: multiple action representation in the frontal lobe. Science 310, 332–336. doi:10.1126/science.1115593.

Nelissen, K., Vanduffel, W., 2011. Grasping-related functional magnetic resonance imaging brain responses in the macaque monkey. J. Neurosci. 31, 8220–8229. doi:10.1523/JNEUROSCI.0623-11.2011.

Neubert, F.-.X., Mars, R.B., Thomas, A.G., Sallet, J., Rushworth, M.F.S., 2014. Comparison of human ventral frontal cortex areas for cognitive control and language with areas in monkey frontal cortex. Neuron 81, 700–713. doi:10.1016/j.neuron.2013.11.012.

Palomero-Gallagher, N., Zilles, K., 2018. Differences in cytoarchitecture of Broca's region between human, ape and macaque brains. Cortex 1–22. doi:10.1016/j.cortex.2018.09.008.

Patriat, R., Molloy, E.K., Meier, T.B., Kirk, G.R., Nair, V.A., Meyerand, M.E., Prabhakaran, V., Birn, R.M., 2013. The effect of resting condition on resting-state fMRI reliability and consistency: a comparison between resting with eyes open, closed, and fixated. Neuroimage 78, 463–473. doi:10.1016/j.neuroimage.2013.04.013.

Petrides, M., Cadoret, G., Mackey, S., 2005. Orofacial somatomotor responses in the macaque monkey homologue of Broca's area. Nature 435, 1235–1238. doi:10.1038/nature03628.

Petrides, M., Pandya, D.N., 2002. Comparative cytoarchitectonic analysis of the human and the macaque ventrolateral prefrontal cortex and corticocortical connection patterns in the monkey. Eur. J. Neurosci. 16, 291–310. doi:10.1046/j.1460-9568.2001.02090.x.

Rizzolatti, G., Camarda, R., Fogassi, L., Gentilucci, M., Luppino, G., Matelli, M., 1988. Functional organization of inferior area 6 in the macaque monkey. Exp. brain Res. 71, 491–507.

Schaeffer, D.J., Gilbert, K.M., Gati, J.S., Menon, R.S., Everling, S., 2019a. Intrinsic functional boundaries of lateral frontal cortex in the common marmoset monkey. J. Neurosci. 39, 1020–1029. doi:10.1523/JNEUROSCI.2595-18.2018.

Schaeffer, D.J., Gilbert, K.M., Ghahremani, M., Gati, J.S., Menon, R.S., Everling, S., 2019b. Intrinsic functional clustering of anterior cingulate cortex in the common marmoset. Neuroimage 186, 301–307. doi:10.1016/j.neuroimage.2018.11.005.

Schaeffer, D.J., Hori, Y., Gilbert, K.M., Gati, J.S., Menon, R.S., Everling, S., 2020. Divergence of rodent and primate medial frontal cortex functional connectivity doi:10.1073/pnas.2003181117, 202003181.

Sharma, S., Mantini, D., Vanduffel, W., Nelissen, K., 2019. Functional specialization of macaque premotor F5 subfields with respect to hand and mouth movements: a comparison of task and resting-state fMRI. Neuroimage 191, 441–456. doi:10.1016/j.neuroimage.2019.02.045.

Shepherd, S.V., Freiwald, W.A., 2018. Functional networks for social communication in the macaque monkey. Neuron 99, 413–420. doi:10.1016/j.neuron.2018.06.027.

Theys, T., Pani, P., van Loon, J., Goffin, J., Janssen, P., 2012. Selectivity for three-dimensional shape and grasping-related activity in the macaque ventral premotor cortex. J. Neurosci. 32, 12038–12050. doi:10.1523/JNEUROSCI.1790-12.2012.

Touroutoglou, A., Bliss-Moreau, E., Zhang, J., Mantini, D., Vanduffel, W., Dickerson, B.C., Barrett, L.F., 2016. A ventral salience network in the macaque brain. Neuroimage 132, 190–197. doi:10.1016/j.neuroimage.2016.02.029.

Vanduffel, W., Fize, D., Mandeville, J.B., Nelissen, K., Van Hecke, P., Rosen, B.R., Tootell, R.B., Orban, G.A., 2001. Visual motion processing investigated using contrast agent-enhanced fMRI in awake behaving monkeys. Neuron 32, 565–577. doi:10.1016/S0896-6273(01)00502-5.

Vijayakumar, S., Sallet, J., Verhagen, L., Folloni, D., Medendorp, W.P., Mars, R.B., 2018. Mapping multiple principles of parietal–frontal cortical organization using functional connectivity. Brain Struct. Funct. 0, 0. doi:10.1007/s00429-018-1791-1.

Vincent, J.L., Patel, G.H., Fox, M.D., Snyder, A.Z., Baker, J.T., Van Essen, D.C., Zempel, J.M., Snyder, L.H., Corbetta, M., Raichle, M.E., 2007. Intrinsic functional architecture in the anaesthetized monkey brain. Nature 447, 83–86. doi:10.1038/nature05758.

Wang, L., LaViolette, P., O'Keefe, K., Putcha, D., Bakkour, A., Van Dijk, K.R.A., Pihlajamäki, M., Dickerson, B.C., Sperling, R.A., 2010. Intrinsic connectivity between the hippocampus and posteromedial cortex predicts memory performance in cognitively intact older individuals. Neuroimage 51, 910–917. doi:10.1016/j.neuroimage.2010.02.046.